# A Conceptual hydrodynamic model of a geological discontinuity in hard rock aquifers: example of a quartz reef in granitic terrain in South India

Benoît Dewandel, Patrick Lachassagne, Faisal K. Zaidi, Subash Chandra

Published in Journal of Hydrology 405 (2011) 474–487

# A Conceptual hydrodynamic model of a geological discontinuity in hard rock aquifers: example of a quartz reef in granitic terrain in South India

Benoît DEWANDEL[1*], Patrick LACHASSAGNE[1,2], Faisal K. ZAIDI[3,4], and Subash CHANDRA[2]

1- BRGM, Water Division, Resource Assessment, Discontinuous Aquifers Unit, 1039 Rue de Pinville, 34000 Montpellier, France; b.dewandel@brgm.fr; (*Corresponding author).

2- Now at Danone Waters France, 11 av. G. Dupas, BP 87, 74503 Evian-les-Bains Cedex, France; Patrick.lachassagne@danone.com.

3- National Geophysical Research Institute, Indo-French Centre for Groundwater Research, Uppal Road, 500 007 Hyderabad, India; schandra75@gmail.com.

4- Now at Department of Geology, College of Science, King Saud University, Riyadh, Kingdom of Saudi Arabia; fk.zaidi@gmail.com.

## Abstract

The structure and hydrodynamic properties of geological discontinuities and of a deeply weathered granite aquifer near these structures are described on the basis of geological, geophysical and hydrodynamic investigations in two sites of South India located along a 20-40-metre-wide quartz reef intruding a weathered Archean biotite granite. One of the two sites also comprises a metre-wide dolerite dyke.

Weathering processes appear to be at the origin of fissures development and of a related enhanced local hydraulic conductivity, both in the quartz reef and in the surrounding granite. The weathering profile in the granite (saprolite and fissured layer) is characterized by an abrupt deepening of the weathered layers in the granite near the contact and in the quartz reef itself. Therefore, the weathering profile shows a 'U'-shape geometry with, among others, the verticalization of the granite's fissured layer. The hydraulic conductivity of this verticalized

layer is on average 5 x $10^{-6}$ m/s and storativity about $10^{-3}$ (-). The hydraulic conductivity of the fissured quartz is 4 to 6 x $10^{-6}$ m/s and its storativity about 3 to 5 x $10^{-4}$ (-). Both media are also characterized by a matrix hydraulic conductivity ($10^{-7}$ to $10^{-9}$ m/s) and by a significant heterogeneity in hydrodynamic properties that generates preferential flow paths along the sub-vertical fissures parallel to the reef axis. A special attention has been paid for characterizing this heterogeneity.

The weathering of the dolerite dyke, however, results in a local low hydraulic conductivity, which consequently does not enhance either the thickness of weathered granite layers or its hydraulic conductivity.

The obtained results complete the conceptual hydrogeological model developed for weathered granite aquifers in characterizing the relationships between weathering processes and hydrodynamic properties near geological discontinuities.

Key words: hard rock, discontinuity, granite, weathering, hydrodynamic properties, heterogeneity in hydraulic conductivity

## 1. Introduction

Hard rocks (plutonic, metamorphic rocks) form part of the basement of continents and, as such, occupy large areas throughout the World (Africa, South and North America, India, Europe, Asia, Australia, etc.). Groundwater resources in aquifers (HRA) are generally low in terms of available discharge per well (from a few to a few tens of $m^3$/h) compared to those from porous, karst, and volcanic aquifers. However, HRA are geographically widespread and thus well-suited for water supply to scattered populations and small to medium-size towns, or suburbs of larger cities. Their groundwater resources largely contribute to economic development, especially in regions exposed to arid and semiarid climatic conditions where surface-water resources are limited as, for example, in Africa and in India (Uhl and Sharma, 1978; Gustafson and Krásný, 1994; Houston and Lewis, 1998). In such regions, HRA commonly are the only available perennial water resource, supplying the population as well as the agricultural and industrial sectors. However, the knowledge of such aquifers, e.g., their geometry, their hydraulic properties, etc., is currently meagre and needs to be improved.

Significant advances have recently been made in the geological and hydrogeological characterization of such complex aquifers (Omorinbola, 1982; Owoade, 1995; Chilton and Foster, 1995; Taylor and Howard, 2000; Lachassagne et al., 2001; Wyns et al., 2004,

Maréchal et al., 2004; Dewandel et al., 2006; Ayraud et al., 2008; Courtois et al., 2010; Lachassagne et al., 2011). These studies show that the geometry and the hydrodynamic properties of HRA mainly result from deep weathering processes of the parent rock. Such processes involve biogeochemical hydrolysis of the minerals constituent of the rocks and their mineral transformation under new surface conditions, mainly into clay-rich materials (Tardy, 1971, 1993, 1998; Nahon, 1991). Additionally, these processes are controlled by the regional geodynamical history, which can lead to multiphase weathering profiles because of alternating erosion and weathering phases (Taylor and Howard, 2000; Dewandel et al., 2006).

In granite-type rocks (e.g. granite, gneiss), a typical weathering profile comprises two main stratiform layers sub-parallel to the paleo-surface contemporaneous of the weathering processes (Fig.1; Chilton and Smith-Carrington, 1984; Chilton and Foster, 1995; Wyns et al., 1999 and 2004, Krásný and Sharp, 2007; Maréchal et al., 2007, and others). From the top downward, they are (i) the **saprolite layer**, a clay-rich material usually characterized by low hydraulic conductivity, and (ii) the fissured layer characterized by dense horizontal fissuring within the first few metres and a depth-decreasing of the sub-horizontal and sub-vertical fissure sets (Howard et al., 1992; Houston and Lewis, 1998; Maréchal et al., 2004; Wyns et al., 2004; Dewandel et al., 2006). This last layer usually assumes the transmissive function of the aquifer. The **underlying unfissured and fresh basement** is only locally permeable where deep fractures occur, but these conductive zones are much less dense than in the overlying fissured layer and their hydrodynamic properties are highly variable (Pickens et al., 1987; Blomqvist 1990; Walker et al., 2001; Kuusela et al., 2003; Cho et al., 2003). Flow can be fractionalized, i.e. controlled by the orientation of the fracture network (Leveinen et al., 1998).

As a consequence, where the formation is not affected by geological discontinuities, such as faults, veins or dykes, and exposed to deep weathering processes, the saprolite and the fissured layers together make up a composite aquifer of up to 100 m thick (Fig.1). Hydrogeologically, this medium can be considered as a multilayer system where each layer is characterized by its own specific and quite homogeneous hydrodynamic properties. This relative “homogeneity” allows several practical applications (Lachassagne et al., 2011), among which aquifer budgeting (Maréchal et al., 2006) or the development of Decision Support Tools (Dewandel et al., 2008, 2010). However, where the granite is intruded by quartz, pegmatite or aplite veins, dolerite dykes, or younger granite, or affected by tectonic faults, the layers geometry and their hydrodynamic properties may substantially differ from

the above-presented conceptual model. Locating such heterogeneities in hard rocks, commonly resulting from lineament analysis and/or geophysical surveys, constitutes the backbone of borehole siting, as major discontinuities and their intersections are often assumed to be strong indicators of a groundwater resource (Mabee et al., 1994; Minor et al., 1995; Sander et al., 1997; Chandra et al., 2006; Sander, 2007). However, such structures do not necessarily give impressive results in terms of well productivity (Sander, 2007); probably because at present their hydrogeological properties in terms of hydrodynamics and geometry are insufficiently understood.

The objective of the present paper is to improve the understanding of the geometry and hydrodynamic properties of such geological discontinuities, through the case-study of a 20 to 40-metre-thick quartz vein intruding granite that was exposed to deep weathering processes. This work has led to a 3-D conceptual hydrogeological model of this structure, on the basis of geological and geophysical surveys, and hydraulic tests carried out on two pilot sites equipped with a total of 21 boreholes (Fig. 2, Maheshwaram area, Ranga Reddy District, Andhra Pradesh, India).

## 2. Geological setting

The studied sites are located 40 km south of Hyderabad (Andhra Pradesh, India). The area is characterized by a relatively flat topography with altitudes ranging from 670 to 590 m above mean sea level. The region experiences a semi-arid climate controlled by the periodicity of the monsoon (rainy season: June to October). Mean annual precipitation is about 750 mm, of which more than 90% falls during the monsoon season.

The area is underlain by Archean biotite granite that is locally intruded by leucocratic granite. These granites are affected by deep in-situ multi-phase weathering-and-erosion processes (Dewandel et al., 2006). At the regional scale, the weathered horizons more or less follow the current topography and, from top to bottom, are composed of:

- A 1-3-m thick layer of sandy regolith, locally capped by a lateritic crust (<50 cm);
- A 10-15-m thick layer of laminated saprolite;
- And, a 15-20-m thick layer of fissured granite, where weathered granite and clay minerals can partially fill the fissures.

The granites are locally intruded by up to 40-m-wide quartz veins (Archean in age) and metre-wide dolerite dykes (2.5 to 1.6 Ga; G.S.I. 2002; Fig. 2). Quartz reefs systematically occupy positive relief in the area. In order to investigate the impact of such discontinuities on the

weathering-profile structure and its hydrodynamic properties, geological and geophysical investigations were carried out on two pilot sites: “IFP 1” and “Kothur” (Figs. 2 and 3). The two sites, separated by 7 km, are located along the same sub-vertical and north-south decametre-wide quartz reef.

Electrical Resistivity Tomography profiles were carried out on the two sites for siting the 21 boreholes used in the study (Chandra et al., 2010). Five ERT profiles were carried on the Kothur site and one on the IFP1 site. All ERT profiles show that the quartz reef, particularly at depth, is characterized by lower resistivities than the surrounding granite, which is attributed to a more developed fissure network at depth (see supplemental material).At Kothur six boreholes were drilled in the central area and in the pinch-out zone of the quartz reef and 5 in the surrounding granite (Fig. 3a and 3b). The ten IFP1 boreholes were located within the granite in the pinch-out zone of the quartz reef and near a metre-wide dolerite dyke (Fig. 3a) that was intersected by two boreholes (IFP 1-4 and 1-8).The depth of the 21 boreholes ranges between 35 and 91.4 m (Table 1); detailed geological logs were prepared from drill cuttings (see supplemental material). At IFP1 site, two pre-existing farmer’s wells (bw1 and bw2, Fig. 3a) drilled within the granite are also present, but their exact depth is unknown.

The combination of the geophysical and the geological data allowed characterizing both the structure of the geological formations and the geometry of the weathering profile near the intrusion. Geological cross-sections perpendicular and parallel to the reef for the two sites clearly show that the weathering profile is significantly deepened near the quartz reef (Figs 4a, b and c). At the outcrop scale, the orientation of major fissures (metre to decametre wide) in the quartz reef was measured (see supplemental material). The fissures are mostly sub-vertical and organized in two main sub-orthogonal sets, one sub-parallel (N000 90°) to the quartz vein and the second sub-orthogonal (N100 90°) to it. A few sub-horizontal fissures were also observed, but due to the relatively flatness of the outcrops their number is probably underestimated. Within the first ten metres from surface, the quartz is highly weathered and densely fissured from centimetre to decametre scale. However, near the contact with the granite, i.e. on the sides of the quartz reef and in the pinch-out zones, this highly weathered and fissured material can reach up to 50 m depth (Figs. 4b and c).Near the quartz reef, the granite is also characterized by an important deepening of the weathering profile. On average, saprolite thickness increases by a factor 1.5 to 3 and the fissured layer by a factor 3 to 5, compared to the zone not affected by the intrusion. Locally, the bottom of the fissured layer can reach more than 70 m depth, whereas farther from the quartz reef the weathering profile in the granite stops at few tens of metres from the surface (Figs. 4).

The IFP1 sub-vertical and metre-wide dolerite dyke sub-parallel to the quartz reef is highly weathered within the first 6 m from the surface (clayey material), then poorly fissured up to 15 m, and finally hard and compact. Near this dyke there is no-evidence of a deepening of the weathering front and of the development of a local deeper fissuring.

Previous studies (Maréchal et al., 2004; Dewandel et al., 2006) showed the relative homogeneity of the hydrodynamic properties of the weathered/fissured hard-rock aquifers where the granite is not affected by such discontinuities. Several questions now arise: are the hydrodynamic properties different in such verticalized weathered-fissured layers? Does the preferential orientation of fissures in the quartz reef play a role? What is the hydrogeological conceptual model of these discontinuities? To try and provide answers to these questions, slug tests and pumping tests were performed on both sites.

# 3. Hydrodynamic investigations

## 3.1. Slug tests

Twenty-one slug tests were carried out in the boreholes of both pilot sites and were interpreted using the Bouwer and Rice (1976) technique for unconfined aquifers with completely or partially penetrating wells. The obtained distribution of hydraulic conductivities constitutes a preliminary estimate of the hydraulic conductivity of the weathered layers in the granite and in the quartz aquifers near the wells (Fig. 5).

Near the quartz reef, the hydraulic conductivity of the fissured granite ranges from $8.5 \times 10^{-8}$ m/s to $8.8 \times 10^{-6}$ m/s with a geometrical mean of $2.4 \times 10^{-6}$ m/s and a standard deviation of 0.6 computed on a logarithmic scale ($\log K_{slug}$: -5.6±0.6). In the quartz reef, values are similar and range from $5.0 \times 10^{-8}$ m/s up to $1.6 \times 10^{-5}$ m/s with a geometrical mean of $2.6 \times 10^{-6}$ m/s and a standard deviation on a log scale of 1.0 ($\log K_{slug}$: -5.6±1.0). Within these distributions, a small population of two boreholes (IFP30-3, $K=8.5 \times 10^{-8}$ m/s and IFP30-6, $K=5.1 \times 10^{-8}$ m/s) with hydraulic conductivities of less than $10^{-7}$ m/s corresponds to poorly fissured granite and quartz and is possibly representative of the matrix hydraulic conductivity. The hydrodynamic properties of the dolerite dyke were not explored since no water contribution was observed during drilling despite the shallow water-table (4 m from surface). The hydraulic conductivity distributions in the quartz reef and in the nearby granite seem to follow near-log normal distributions, similar to that of the stratiform fissured layer far from discontinuities in the same granite (geometric mean of $4.4 \times 10^{-6}$ m/s, Maréchal et al., 2004). However, the spatial distribution of hydraulic conductivity in the quartz reef is highly variable and is closely linked

198 with the degree of weathering. Indeed, at the centre of the quartz reef, where a high grade of
199 weathering and fissuring only affects the first metres below surface, the quartz is
200 characterized by quite low hydraulic conductivities (IFP30-1, 30-6; $K<5 \times 10^{-7}$ m/s), whereas
201 it is significantly more permeable near the contact with granite (e.g., IFP30-9, 30-10, 30-11;
202 $K>10^{-5}$ m/s). This shows that most of the conductive fissures develop in the contact zones (i.e.
203 sides and pinch-out zones), whereas the heart of the reef is poorly fissured.
204 For the granite, no clear relationship between hydraulic conductivity and location relative to
205 the quartz reef is found, suggesting that both near and far from the discontinuity the fissured
206 layer of the granite exhibits similar properties.
207
208 ## 3.2. Pumping tests
209 ### *3.2.1. Brief description of the method used*
210 The interpretation of pumping tests in such fissured aquifers commonly is a difficult task, as
211 groundwater flow can be fractionalized (Black, 1994; Le Borgne et al., 2004) and controlled
212 by the hydraulic conductivity of fissures, their density and orientation, and also their
213 relationships with low-hydraulic-conductivity blocks or matrix (e.g. Maréchal et al., 2004; Le
214 Borgne et al., 2006). In order to reveal the various aspects of the hydrodynamic properties of
215 such a complex medium and to appropriately model the pumping test, a special attention has
216 been paid to diagnosing of the tests prior to their modelling. Diagnoses were based on the
217 analysis of derivative drawdown curves on log-log plots that allows flow-regime
218 identification (Bourdet et al., 1983, 1989; Ehlig-Economides, 1988; Spane and Wurstner,
219 1993, Renard et al., 2009). The tests were then interpreted with WinISAPE (BRGM software)
220 and WTFM (Lods and Gouze, 2004).Table2 presents the main characteristics of the pumping
221 tests.
222 The observations and models were visually matched on both drawdown and derivative curves.
223 The sensitivity of the hydrodynamic-parameter estimates was inferred from several fitting
224 tests: it is less than 15% on average for the hydraulic conductivity and less than 20% on
225 average for storativity. Since 34 curves were interpreted for the study, only a few curves are
226 presented here (Fig. 6a, b and c).
227
228 ### *3.2.2. Pumping tests at the Kothur site*
229 Three non-simultaneous pumping tests were performed, two within the quartz reef (IFP30-5
230 and IFP30-10) and one within in the stratiform fissured layer of the granite (IFP30-4) at a
231 quite large distance from the quartz vein (Fig. 3b; Tables 3 to 5).

Pumping in IFP30-5 revealed spherical flow during the early stage of pumping (–1/2 slope of derivative curve; t<100 min; Fig. 6a) that is typical of a borehole partially penetrating the aquifer. As this well intersects about 30 to 40 m of fractured quartz (Fig. 4c), this diagnosis suggests that IFP30-5 is located in a zone where the aquifer is relatively thin compared to where the drawdown progresses. This is corroborated by the geological observations, which show that the thickness of the weathered/fissured zone increases up to 70 m depth north of the site (Fig. 4c). The whole data set from pumping and observation wells has been interpreted with the Hantush model (partially penetrating aquifer with vertical anisotropy in hydraulic conductivity; Hantush, 1961; Fig. 6a). Estimated hydrodynamic parameters are of the same order of magnitude and relatively close from one well to the next with, however, a variability in the estimates and particularly those for hydraulic conductivity and storativity (Table 3); this point will be discussed later. On average, the hydraulic conductivity is $4.0 \times 10^{-6}$ m/s, the storativity about $3.2 \times 10^{-4}$ (-) and the aquifer thickness is estimated to be about 100 m. The computed aquifer thickness appears slightly overestimated compared to reality (about 70 m), which we explain by the uncertainty of the real productive length in wells (screened thickness on Table 3) but also by the use of the Hantush model that considers a well that partially penetrates the aquifer whereas IFP30-5 is located in a pinch-out zone of the aquifer. The vertical anisotropy ratio in hydraulic conductivity (Kx/Kz) is about 3 and probably reveals a depth-decreasing hydraulic conductivity due to a depth-decreasing density of fissures.

The test performed in IFP30-10 revealed a dual porosity behaviour (Fig. 6b). The overall data set has thus been interpreted with a dual porosity model. Two observation wells (IFP30-6 and 30-7) were interpreted in the matrix, the others being in the fissure network (Table 4; Fig. 6b). Compared to the previous pumping test, spherical flow is absent showing that IFP30-10 intersected most of the aquifer thickness and thus that the bottom of the aquifer is close to 70 m deep. The estimated hydrodynamic parameters are consistent with the ones obtained in IFP30-5 and of the same order of magnitude (Table 4). This test gives complementary information on the hydraulic parameters of the quartz reef aquifer. On average, the hydraulic conductivity of the aquifer is $6.2 \times 10^{-6}$ m/s, the storativity is about $4.6 \times 10^{-4}$ (80% in the matrix and 20% in the fissures), and the matrix hydraulic conductivity is about $2.4 \times 10^{-9}$ m/s. Variability in hydraulic conductivity and storativity estimates was also noted and will be discussed later.

The third test at Kothur (IFP30-4) characterises the stratiform fissured layer of the granite not affected by the reef. Only two observation wells reacted to the test (IFP30-7 and 30-8). The aquifer behaviour is typical of a dual-porosity medium and the hydrodynamic parameters are

very similar (Table 5). The hydraulic conductivity of the fissured granite is on average 6.4 x $10^{-6}$ m/s, the storativity is about 7.2 x $10^{-3}$ (98% in the matrix, 2% in the fissures), and the matrix hydraulic conductivity is about 3.0 x $10^{-9}$ m/s.

### *3.2.3. Pumping tests at the IFP1 site*

At the IFP1 site, wells were drilled in the granite, in the pinch-out zone of the quartz reef (Fig. 3a). A pumping test in IFP1-6 revealed the channelized structure of the aquifer after a few minutes of pumping (1/2 slope of the derivative curve on Fig. 6c). This is consistent with the geological information and particularly the 'U'-shape geometry of the aquifer (Fig. 4a). Therefore, a Theis model combined with two parallel no-flow boundaries was used for the interpretation (Fig. 6c). Several hypotheses were tested for the orientation of the two no-flow boundaries. The best result, which was constrained by the modelled drawdowns for the 10 wells, was obtained for a direction sub-parallel to the quartz reef (N195). Aquifer parameters are quite homogeneous (Table 6) with, however, a certain variability in the hydraulic conductivity and storativity values. The average hydraulic conductivity is 4.5 x $10^{-6}$ m/s and the average storativity 7.8 x $10^{-4}$ (-). Distances from IFP1-6 to the two no-flow boundaries are on average 20 and 44 m respectively, which is consistent with the geological information (Fig. 4a). The nearest no-flow boundary, located east of IFP1-6 (d1=19.5±9 m), corresponds to the dolerite dyke while the farthest boundary is the western limit of the verticalized fissured layer of the granite (d2=44.3±2 m).

Nevertheless, some discrepancies to this overall interpretation are found. Interpretation of the observation well IFP1 data gives higher distances to limits, and particularly to the farthest one (138 m) because of the very low storage coefficient computed for this well (S=7 x $10^{-5}$; dist.limit=1.5$[Tt/S]^{1/2}$; Jacob, 1947). This low value compared to the average found for the site is probably caused by a highly conductive zone connecting this well to the pumping well thus enhancing a rapid pressure transfer between the two wells, quicker than the general one found at the site scale. The re-computation of the distance to limits with the average storage coefficient found at the site scale gives results that are consistent with the ones found in the other wells (Table 6). Compared to other wells, drawdown at IFP 1-3, 1-4 and 1-8 was very low (<0.8 m) which is explained by their location outside the permeable channel (Figs. 3a and 4a). The data were interpreted with the Theis model, but the estimated hydraulic parameters, K and S, are non-realistic and differ by several orders of magnitude from the ones obtained in other wells. These wells are thus located in an aquifer that is poorly connected to the

299 permeable channel. These records nevertheless show that the dolerite dyke no-flow boundary
300 is not a completely impervious limit, but rather a low-permeability barrier.
301 The second test performed in IFP1-8 produced drawdown in only a few observation wells
302 (IFP1-4 and farmer wells BW1 and 2; Fig. 3a). The eight other observation wells did not react
303 to pumping, corroborating the presence of a no-flow boundary between IFP1-8 and IFP1-5,
304 i.e. the dolerite dyke. This test reinforces the scheme deduced from the test at IFP1-6. The
305 interpretations give similar results, with an average hydraulic conductivity of the aquifer at
306 $1.5 \times 10^{-5}$ m/s and a storativity, S, of about $2.2 \times 10^{-4}$ (-).
307

308 ## 3.3. Anisotropy and heterogeneity in hydraulic conductivity

309 Fissure measurements on the quartz-reef outcrops at IFP1 and Kothur sites show that the
310 fissure network is well organized with dominant sets that are sub-parallel and sub-orthogonal
311 to the reef axis (see supplemental material). Moreover, the variability in hydraulic
312 conductivity - particularly within the quartz reef ($\log K_{slug}$: -5.6±1.0) - is high because of the
313 variation in the weathering grade. As a consequence, anisotropy and heterogeneity in
314 hydraulic conductivity are expected and may explain the variability in hydraulic conductivity
315 and storativity deduced from the pumping tests.
316

317 ### 3.3.1. Homogeneous and anisotropic aquifer: the stratiform horizontal fissured layer

318 In an ideal homogeneous and anisotropic aquifer, the hydraulic conductivity on the horizontal
319 plane can be represented by a tensor characterized by two orthogonal major and minor axes.
320 When a pumping test is performed, the drawdown geometry forms an ellipse that reflects the
321 anisotropy ratio (Hantush, 1966; Hantush and Thomas, 1966; Ramey, 1975; Neuman et al.,
322 1984). The estimation of the anisotropy ratio and of the major and minor hydraulic
323 conductivity orientations requires several observation wells located at various angle from the
324 two anisotropy axes (e.g. Neuman et al., 1984). For such a medium and considering an
325 isotropic storativity, drawdown curves from observation wells will all be characterized by the
326 same semi-log slope (Jacob's straight-line), regardless of the distance to the pumping well,
327 leading to equal estimated transmissivity or hydraulic conductivity values for each
328 observation well. Only the intercept of the straight line with the time axis will differ because
329 the anisotropy terms are only incorporated in the well-function (or within the log term for the
330 Jacob's approximation). The analytical solutions used here start (Theis + two no-flow
331 boundaries) or end (Hantush and dual porosity) with radial flow (straight-line on semi-log
332 diagram), suggesting that in the scheme of an ideal anisotropic aquifer the hydraulic

conductivity estimates for a particular pumping test should be the same or very close between wells. Such a statement is valid for the test performed at IFP30-4 in the horizontal stratiform fissured granite far from the quartz reef, where observation wells are laid out at right angles ($K\_30\text{-}4 \approx K\_30\text{-}8 \approx K\_30\text{-}3 \approx 6.4 \times 10^{-6}$ m/s; Table 5). In addition, the estimated storativity for the two observation wells is very close ($7\text{-}8 \times 10^{-3}$), indicating an anisotropy ratio near 1 when using the earlier mentioned anisotropic model. This suggests that at IFP30-4 the stratiform horizontal fissured layer is neither affected by a significant anisotropy in hydraulic conductivity onto the horizontal plane, nor affected by significant heterogeneities in hydraulic conductivity at the pumping-test scale. However, this information should be confirmed by one or more additional observation wells in other directions, or by additional tests in one of the two observation wells (Neuman et al., 1984).

### 3.3.2. Heterogeneous and anisotropic aquifer: verticalized fissured granite and quartz

In the quartz reef (tests in IFP30-5 and IFP30-10) and in the granite at the pinch-out zone of the reef (IFP1-6), the estimated hydraulic conductivity differs between wells with a factor between 3 and 5 (Tables 3, 4 and 6). This implies that the tested aquifers are not ideal anisotropic aquifers or/and are affected by significant heterogeneity in hydraulic conductivity as illustrated by the analysis of slug-test data (Fig. 5).

Based on synthetic aquifers with heterogeneous transmissivity and homogeneous storativity, Meier et al. (1998) and Sánchez-Vila et al. (1999) showed that for long-duration tests the transmissivity values obtained with the Jacob straight-line method on observation wells at various distances from the pumping well are almost identical to the average transmissivity of the medium, even if the heterogeneity in transmissivity is important. However, storativity estimates vary considerably which, according to these works, is a result of the heterogeneity in transmissivity. Our aquifer hydraulic conductivity and storativity data set can be interpreted similarly: the used methods provide representative hydraulic conductivity values of the aquifers since K estimates are comparable, and the high variability in storativity estimates, which can be about an order of magnitude for the same test, may be the consequence of a heterogeneous hydraulic conductivity field. According to Meier et al. (1998) and Sánchez-Vila et al. (1999), a well located in a high hydraulic-conductivity zone compared to the estimated one, results in an overestimated storativity value, and vice versa. Furthermore, the obtained transmissivity depends not only on the transmissivity values along the connecting path, but also on the average transmissivity values of the full domain (Sánchez-Vila et al., 1999). With our data set, no correlation between slug-test data and storativity was found,

probably because of the very local estimation assigned to this method (slug tests have an action radius of a few metres around the well). Strong increases of the transmissivity variability of these numerical models, which was introduced by increases in the variance transmissivity fields, produced ellipsoidal shapes of estimated transmissivity around the pumping well, which were even better defined when the highest transmissivity zones were connected by highly permeable fractures. Even though these shapes may be exaggerated due to numerical artefacts, they seem nevertheless related to the transmissivity field. This point was, however, not discussed by the authors.

### 3.3.3. Proposed methodology for identifying the major and minor axes in hydraulic conductivity and results

In order to understand the variations in hydraulic conductivity estimated from one well to another, we prepared graphs representing the hydraulic conductivity values obtained at each observation well on the X-Y plane (K values from Tables 3, 4 and 6). If hydraulic conductivity estimates depend upon the hydraulic conductivity values along the connecting path between the pumping well and the observation well as well as on the average hydraulic conductivity value at the pumping test scale, one may expect variations in estimated values according to the direction between the pumping well and the observation well.

The hydraulic conductivity estimated in a particular observation well (*Kobs.well*) is plotted as a function of the angle $\beta$ between the geographical north (reference axis) and the pumping-well / observation-well direction. Each *Kobs.well* is thus defined by two components, $K_E$ representing the projection onto the east-west or X-axis ($K_E = Kobs.well x Cos\beta$) and $K_N$, the projection onto the north-south or Y-axis ($K_N = Kobs.well x Sin\beta$). The pumping well is located at the centre of the graph.

The three tests where the method was applied (Figs. 7a, b and c) clearly show correlations between the estimated hydraulic conductivity and the orientation of the well to the pumping well. Regardless of the distance between pumping well and observation well, the plotted hydraulic conductivities describe ellipses showing that the hydraulic conductivities obtained along the reef axis are systematically larger than the orthogonal estimates. Higher values are explained by the velocity at which the drawdown propagates, which depends upon the hydraulic diffusivity ($D = K.b/S$; $b$ being the aquifer thickness). Because the variability in hydraulic conductivity is usually much larger than the storativity one, diffusivity is thus large for highly conductive zones and small for low-conductivity zones. Thus, when pumping, a

vertical hydraulic gradient from lower to higher conductive zones is induced, which means that the highly conductive fissures or the fissure network that is best connected to the pumping well can be regarded as drainage structures or as lateral extensions of the well (Schad and Teutsch, 1994).

Hydraulic conductivity ellipses are defined by major and minor axes (*Kmax* and *Kmin)* and are supposed to characterize an average pseudo or apparent anisotropy introduced by the heterogeneity in hydraulic conductivity of the aquifer, or, in the case of fractured media, the variability in hydraulic connectivity with the different well locations; $\alpha$ representing the angle between the Y-axis and *Kmax*. The ratios *Kmax/Kmin* are comparable, between 2.6 and 3.1, and reveal the degree to which the fissures in the two orthogonal orientations are connected; however, the ratio values were not interpreted in a quantitative sense. To agree with previous work - the evaluated hydraulic conductivity at the pumping well should be representative of the whole heterogeneous medium (Meier et al., 1998) - but also to validate the analysis, the hydraulic conductivity estimated for the pumping well should represent the average hydraulic conductivity of the aquifer and should be close to the average hydraulic conductivity value deduced from this analysis ($K_{mean}=[Kmax \, . \, Kmin]^{0.5}$). Using such an approach, $K_{mean\_30\text{-}10}$=5.9 x$10^{-6}$ m/s is compared to $K_{IFP30\text{-}10}$= 6.3 x $10^{-6}$ m/s, $K_{mean\_30\text{-}5}$=3.6 x$10^{-6}$ m/s to $K_{IFP30\text{-}5}$= 4.2 x $10^{-6}$ m/s, and $K_{mean\_1\text{-}6}$=5.1 x$10^{-6}$ m/s to $K_{IFP1\text{-}6}$= 5.1 x $10^{-6}$ m/s. Differences are thus small, between 0 to 15%, compared to the ones obtained from pumping wells. However, the ellipses are mismatched in a few points. Some lie outside the ellipse, such as IFP1-1, which suggests that the pressure transfer is easier between this well and the pumping well due to a preferential flow path as previously suggested, or they lie inside the ellipse due to a lower conductive zone (IFP30-8, IF30-7; Fig. 7b).

From this analysis, it results that the major ellipse axes are clearly oriented sub-parallel to the quartz reef. Consequently, for the tests in the quartz reef, it can be concluded that the sub-vertical fissure set parallel to the reef axis ensures a preferential connection between the pumped and the other wells. However, at right angles to the reef the connection is lower, most probably because of the variation in the degree of fissuring between the heart and the side of the reef.

In the verticalized fissured layer at the quartz vein pinch-out zone (Fig. 7c), we also find variability in the connectivity of the fissure network. The major axis is also sub-parallel to the sub-vertical fissure set and parallel to the reef axis. This result suggests that in the pinch-out zone of the quartz reef, and probably also at the contacts on the eastern and western sides, the verticalized fissured granite is affected by a dominant set of sub-vertical conductive fissures

sub-parallel to the reef. This feature differs from the classic stratiform horizontal fissured layer, where horizontal conductive fissures dominate (Fig. 1; Maréchal et al., 2004).

# 4. HYDROGEOLOGICAL CONCEPTUAL MODEL OF THE QUARTZ REEF

Geological, hydrogeological and geophysical investigations performed along the quartz reef allow completing the understanding of the structure and the hydrogeological properties of hard-rock aquifers exposed to deep weathering processes (Fig. 8).

## 4.1. Aquifer geometry

Near the quartz reef the weathering fronts within the granite (e.g. bottom of saprolite and of the fissured layer) are noticeably deeper compared to the classic stratiform weathering profile. On average, the thickness of the saprolite increases by a factor of 1.5 to 3 and that of the fissured layer by a factor of 3 to 5. Near the contact, the geometry of the weathering profile in the granite is, as for the classic stratiform weathering profile, characterized by two sub-parallel layers: the saprolite and the fissured layers. However, they are not sub-parallel to the paleo-surface contemporaneous with the weathering, but sub-parallel to the discontinuity borders. As a result, the weathering profile exhibits a 'U' shape composed of parallel layers. The quartz reef is characterized by mainly sub-vertical fissures that are sub-parallel and sub-orthogonal to the reef axis. The top layer is highly fissured and weathered and the fissure density rapidly decreases with depth. Density in fissuring and the grade of weathering vary also in space and are more pronounced at the contact with granite, i.e. on the sides and in the pinch-out zones, than at the heart of the vein. This 'U' shape of the weathering layers results from similar processes as those observed in horizontal stratiform weathering profiles:

(*i*) The constraints resulting from the development of the weathering profile in the granite surrounding the quartz reef induce fissuring of the quartz reef. This explains the numerous metre- to decametre-wide fissures observed in the quartz reef outcrops. Constraints in the granite are induced by the swelling of some minerals, particularly biotite (Wyns et al., 1999, 2004; Lachassagne et al., 2011);

(*ii*) This weathering-induced fissuring enhances water circulation and in return favours a local deepening of the weathering fronts in the granite near the contact with the quartz reef. The lower strain is thus deviated in the direction of the discontinuity, which favours

the development of a verticalized fissured layer in the granite at the contact with the reef. This point is supported by the heterogeneity in hydraulic conductivity, which shows evidence that this layer is characterized by dominant conductive fissures sub-parallel to the intrusion

(*iii*) The induced weathering favours deeper fissures in the quartz vein, and so on.

Thus, during the weathering of granitic formations such a discontinuity favours a local deepening of the weathering fronts in the host rock and thus favours a thickening of the transmissive part of the aquifer (the fissured layer). In addition, the quartz vein is also subject to weathering. It causes small-scale fissures that further enhance the hydraulic conductivity. This *in situ* weathering amplifies the above-described process.

Intrusives or veins whose weathering products are of low permeability, such as those of dolerite dykes, do not favour water circulation, neither in their heart, nor around them. The stratiform weathering profile of the neighbouring granite thus remains undisturbed. Moreover, such dykes —as in the case of the IFP1 site— act as low-permeability barriers that compartment the horizontal fissured layer.

## 4.2. Hydrodynamic properties of the aquifer

### *4.2.1. Granite near the contact with the discontinuity*

Far from the quartz reef, the stratiform horizontal fissured layer of the granite is characterized by quite homogenous hydrodynamic parameters (pumping tests in IFP1-8 and IFP30-4): the hydraulic conductivity is about $10^{-5}$ m/s and the storativity ranges between 0.2 and $7 \times 10^{-3}$. These values are similar to the ones found in the same area: $K=5 \times 10^{-5}$ m/s and $S= 6 \times 10^{-3}$, (Maréchal et al., 2004), and $K=1.6 \times 10^{-5}$ m/s (Dewandel et al., 2006). As previously shown by Maréchal et al. (2004), the granite is characterized by dual-porosity behaviour, being affected by sub-horizontal and sub-vertical fissure networks and low-permeability blocks with a hydraulic conductivity of about $3 \times 10^{-9}$ m/s. In addition, the two fissure sets induce a significant horizontal anisotropy in permeability ($K_{horiz.}/K_{vert.}$: 10) because of the well-developed horizontal conductive fissure network. The pumping test performed in IFP1-8 within the horizontal fissured layer did not show such behaviour as a result of the presence of the low-permeability dolerite dyke which became apparent at the early stage of the pumping and masked the dual-porosity behaviour.

The average hydraulic conductivity of the verticalized fissured layer along the quartz reef is about $4.5 \times 10^{-6}$ m/s, and the average storage coefficient $7.8 \times 10^{-4}$ (-). The similarity between these values and the ones from the 'classic' stratiform horizontal fissured layer in the area

suggests that the conductive zones of both horizontal and verticalized fissured layers have a similar origin, i.e. weathering processes. As in the case of the IFP1-8 test, the two no-flow-boundaries that appear at the early stage of pumping in IFP1-6 probably masked the dual-porosity behaviour of the verticalized granite. However, this layer may also behave like such a medium, as suggested by the low local hydraulic-conductivity values derived from slug tests, 1 to 4 x $10^{-7}$ m/s (IFP30-3 and IFP1-3), which are typical of the hydraulic conductivity values in the block as given by Maréchal et al. (2004). Thus, the verticalized fissured layer of the granite along the contact with the reef is formed by a conductive fissure network (4.5 x $10^{-6}$ m/s) and possibly by low-permeability blocks (about $10^{-7}$ m/s). In addition, this verticalized layer is characterized by a dominant set of conductive fissures that are sub-vertical and sub-parallel to the reef axis (Ky>Kx). This result differs from the 'classic' horizontal fissured layer, where no significant anisotropy was found in the horizontal plane (Kx≈Ky at IFP30-4) and where a conductive sub-horizontal fissure network dominates ($K_x/K_z$=10; Maréchal et al., 2004).

### *4.2.2. Quartz aquifer*

The fissured quartz is characterized by a dual-porosity behaviour; the average hydraulic conductivity of the fissure network is 4 to 6 x $10^{-6}$ m/s, storativity being 3 to 5 x $10^{-4}$ and mainly ensured by low-permeability blocks (2.4 x $10^{-9}$ m/s). However, hydrodynamic properties in the quartz are highly variable in space and closely depend upon the grade of weathering and fissuring: it is poorly fissured with low permeability in the heart and highly conductive at the contact with granite due to an enhanced fissuring. The fissured quartz is also characterized by anisotropy onto the vertical plane, $K_x/K_z$: 3, which is attributed to a decreasing density with depth of the conductive fissures. As for the verticalized fissured layer of the granite, conductive fissures that are sub-vertical and sub-parallel to the reef dominate in the quartz, inducing a higher hydraulic conductivity parallel to the reef (Ky>Kx); however, the anisotropy in hydraulic conductivity could not be estimated.

Even if at Kothur site the aquifer also has a 'U' shape, hydraulic tests do not show evidence of channelized groundwater flow. This is explained by the fact that during the tests the groundwater level was very shallow (4 to 5 m deep) whereas it was more than 15 m deep at the IFP1 site. As a consequence, at Kothur the 'U'-shape aquifer was still well-connected to the surrounding horizontal stratiform fissured layer of the granite aquifer, giving the impression of an infinite aquifer while at the IFP1 site only the 'U' shape aquifer contributed to pumping.

## 5. CONCLUSIONS

The obtained results complement the conceptual hydrogeological model developed for granite aquifers (Taylor and Howard, 2000; Maréchal et al., 2004; Dewandel et al., 2006) in places where geological discontinuities disturb the weathering profile.

Near the quartz reef, weathering processes appear to be at the origin of an enhanced local hydraulic conductivity both in the vein and in the surrounding granite. The quartz reef and the accompanying verticalized fissured granite layer at the contact constitute a composite aquifer characterized by a 'U'-shaped geometry that acts as a local drain. This higher permeability is probably at the origin of the sharp deepening of the weathering front in the surrounding granite and in the quartz reef itself. Hydrodynamic properties of the verticalized fissured granite are comparable to those found in the classic horizontal fissured layer. However, the anisotropy in hydraulic conductivity is reversed as sub-vertical fissures control the groundwater flow at the discontinuity, while fluxes in the classic horizontal fissured layer are mostly controlled by a dominant set of sub-horizontal fissures.

Where the weathering can propagate downward, other geological discontinuities such as deep fractures, leucocratic dykes, pegmatite, or contacts between different geological formations, may also constitute local structures with similar aquifer properties as those described here. As a result, the weathering front should also form a 'U' shape depending upon how vertical the discontinuity is and on the duration of the weathering processes. Such types of structures, searched for and observed by hydrogeologists and geophysicists for borehole siting (e.g. Sander, 2007) are commonly attributed to "tectonic fracturing" ("fault gouges"). The novelty here is to show that the geometry of the aquifer and its hydrodynamic properties are inherited from deep and local *in situ* weathering processes, but are unrelated to tectonic activity. Therefore, where this deepening of the weathering front has developed such structures may be valuable targets for borehole siting, particularly because of the enhanced transmissivity due to an increase in aquifer thickness. However, the permeability of such structures is highly variable in space, being low in the heart and high at the contacts. Such contrasting hydrodynamic properties, and also the more or less important development of the weathering profile along these structures, may explain the high variability of well yields using a standard approach based only on the study of lineaments. Thus, lineament studies combined with structural studies of the weathering profile would improve the chances of siting productive wells. At the opposite, discontinuities that produce weathering material of low permeability,

568 such as dolerite dykes, do not locally enhance the thickness of weathered layers in granite or
569 its hydraulic conductivity, making such structures unfavourable targets.
570 Numerical issues, both for modelling the evolution of the weathering profile along such
571 discontinuities and for modelling of the tests, as well as additional hydraulic tests to assess
572 preferential flow paths (flowmeter tests), to pursue the quantification of heterogeneity in
573 hydrodynamic properties in relation to underground reality (fissures orientation, structure of
574 the weathered layers), are topics of interest for future research. In addition, the development
575 of new analytical solutions for the interpretation of pumping tests in such media would help in
576 improving their characterization, such as including anisotropy, channelized flow and/or the
577 influence of surrounding aquifers.
578 Finally, because of the complex structures and associated properties of such aquifers, special
579 attention has to be paid to water management. The channelized or fractionalized patterns of
580 the flow paths have strong implications in terms of contaminant transport and for delineating
581 appropriate protection perimeters for water-supply wells. Efforts should thus be made for
582 improving the hydrogeological and hydrogeochemical characterization of these aquifers to
583 ensure their safe and sustainable groundwater exploitation. The methods for characterizing the
584 aquifer used here could be used and improved for achieving this goal.
585

586 ## Acknowledgements

587 The authors are grateful to the research-sponsorship from BRGM (France), the Embassy of
588 France in India, ,NGRI (India) and from the French National Research Agency (ANR) under
589 the VMCS2008 program (SHIVA project n°ANR-08-VULN-010-01). Colleagues from NGRI
590 and BRGM are thanked for their fruitful comments, discussions and technical assistance in
591 the field. The three anonymous Journal referees are thanked for their useful remarks and
592 comments that improved the quality of the paper. We are grateful to Dr. H.M. Kluijver for
593 revising the English text.
594

## References


Ayraud, V., Aquilina, L., ; Labasque, T., Pauwels, H., Molenat, J., Pierson-Wickmann, A.C., Durand, V., Bour, O., Tarits, C., Le Corre, P., Fourre, E., Merot, Pj. and Ph. Davy, 2008. Compartmentalization of physical and chemical properties in hard-rock aquifers deduced from chemical and groundwater age analyses. *Applied Geochemistry*, 2008, vol. 23 (9), 2686-2707.

Black, J.H. 1994. Hydrogeology of fractured rocks – a question of uncertainty about geometry, *Applied Hydrogeology*, 3, 56-70.

Blomqvist, R.G. 1990. Deep groundwater in the cristalline basement in Finland, with implications for waste disposal studies. *Geologiska Foereningen i Stockholm Foerhandlingar*, vol.112(4), pp.369-374.

Bourdet, D., Whittle T.M., Dougals, A.A. and Y.M. Pirard. 1983. A new set of type curves simplifies well test analysis, *World Oil*.

Bourdet D., Ayoud J.A. and Y.M. Pirard. 1989. Use of pressure derivative in well-test interpretation. *SPE*, 293-302.

Bouwer, H. and Rice R.C. 1976. A slug test for determining hydraulic conductivity of unconfined aquifers with completely or partially penetrating wells. *Water Resources Research*, 12, 3, 423-428.

Chandra, S., Rao, V.A., Krishnamurthy, N.S., Dutta S., and Ahmed, S., 2006. Integrated studies for characterization of lineaments to locate groundwater potential zones in hard rock region of Karnataka, India. *Hydrogeology Journal*, 14(5), 767-776.

Chandra S., Dewandel B., Kumar D., Dutta S. Bhat A.N., Murthy N.S.K. and S. Ahmed. 2010. Geophysical Characterization of Quartz Reef Intrusive Lineaments in Granite Hard Rock for Groundwater Occurrences, Applied Geophysics, in press.

Chilton, P.J., and Foster, S.S.D. 1995. Hydrogeological characterization and water-supply potential of basement aquifers in tropical Africa. *Hydrogeology J.*, *3*(1), 36-49.

Chilton, P.J. and Smith-Carrington, A.K. 1984. Characteristics of the weathered basement aquifer in Malawi in relation to rural water supplies. Challenges in African Hydrology and Water Resources, proc. Harare Symposium, July 1984, pp.57-72.

Cho M., K-M. Ha, Y-S. Choi, W-S. Kee, P. Lachassagne and R. Wyns. 2003. Relationship between the permeability of hard-rock aquifers and their weathered cover based on geological and hydrogeological observation in South Korea. IAH Conference on "Groundwater in fractured rocks", Prague 15-19 September 2003, Prague.

628 Courtois, N., Lachassagne, P., Wyns, R., Blanchin, R., Bougaïré, F.D., Somé, S. and A.
629 Tapsoba. 2010. Country-scale hydrogeological mapping of hard-rock aquifers and its
630 application to Burkina Faso, *Ground Water*, in press.

631 Dewandel B., Lachassagne P., R.Wyns, Maréchal J.C. and N.S. Krishnamurthy, 2006. A
632 generalized hydrogeological conceptual model of granite aquifers controlled by single
633 or multiphase weathering. *Journal of Hydrology*, 330, 260-284,
634 doi:10.1016/j.jhydrol.2006.03.026.

635 Dewandel, B., Perrin, J., Ahmed, S., Aulong. S., Hrkal, Z., Lachassagne, P., Samad, M., S.
636 Massuel. and A. Mukherji. 2008. Management of the groundwater resources in semi-
637 arid hard rock regions under variable water demand and climatic conditions:
638 development of a Decision Support Tool. Groundwater & Climate in Africa
639 International Conference, Kampala, Uganda June 24-28.

640 Dewandel, B., Perrin, J., Ahmed, S., Aulong. S., Hrkal, Z., Lachassagne, P., Samad, M. and
641 S. Massuel. 2010. Development of a Tool for managing groundwater resources in
642 semi-arid hard rock regions. Application to a rural watershed in South India.
643 *Hydrological Processes*, in press.

644 Ehlig-Economides, C.A. 1988. Use of the Pressure Derivative for Diagnosing Pressure-
645 Transient Behavior, *Journ. of Petroleum Technology*, oct.1988.

646 G.I.S., 2002. Geological Survey of India. Geological map: Hyderabad quadrangle – Andhra
647 Pradesh.

648 Gustafson, G. and J. Krásný. 1994. Crystalline rock aquifers: their occurrence, use and
649 importance, *Applied Hydrogeology*, 2, 64-75.

650 Hantush, M.S. 1961. Aquifer tests on partially penetrating wells. *Proc. of the Am. Soc. of*
651 *Civil Engineers*, 87, 171-195.

652 Hantush M.S. 1966. Analysis of data from pumping tests in anisotropic aquifers. J.
653 Geophys. Res., 72, 1709-1720.

654 Hantush M.S. and R.G. Thomas. 1966. A method for analyzing a drawdown test in
655 anisotropic aquifer. *Trans. Am. Geophys. Union*, 36, 281-285.

656 Houston, J.F.T., and R.T. Lewis. 1988. The Victoria Province drought relief project, II.
657 Borehole yield relationships. *Ground Water, 26*(4), 418-426.

658 Howard, K.W.F., M. Hughes, D.L. Charlesworth, and G. Ngobi. 1992. Hydrogeologic
659 evaluation of fracture permeability in crystalline basement aquifers of Uganda.
660 *Applied Hydrogeology, 1*, 55-65.

661 Jacob, C.E., 1947. Drawdown test to determine effective radius of an artesian well, *ASCE*
662 *Trans.*, 112(232), 1047-1064.

663 Krásný J. and J. Sharp, 2007. Hydrogeology of fractured rocks from particular fractures to
664 regional approaches : state-of-the-art and future challenge. In: Krásný J. – Sharp J.M.
665 (eds.): *Groundwater in fractured rocks, IAH Selected Papers*, 9, 1-30. Taylor and
666 Francis.

667 Kuusela-Lahtinen, A., Niemi, A. and Luukkonen, A. 2003. Flow dimension as an indicator
668 of hydraulic behaviour in site characterization of fractured rock. *Ground Water*,
669 vol. 41 (3), pp.33-341.

670 Lachassagne, P., B. Dewandel B., R. Wyns. 2011. The fracture permeability of Hard Rock
671 Aquifers is due neither to tectonics, nor to unloading, but to weathering processes.
672 *Terra Nova, 23*, 145-161.

673 Lachassagne, P., R. Wyns, P. Bérard, T. Bruel, L. Chéry, T. Coutand, J.F. Desprats, and P.
674 Le Strat. 2001. Exploitation of high-yield in hard-rock aquifers: Downscaling
675 methodology combining GIS and multicriteria analysis to delineate field prospecting
676 zones. *Ground Water, 39*(4), 568-581.

677 Le Borgne, Bour, O., de Dreuzy J.R., Davy, P. and F. Touchard. 2004. Equivalent mean
678 flow models for fractured aquifers: insights from a pumping tests scaling
679 interpretation. *Water Res. Research*, 40, W03512, 1-12.

680 Le Borgne, Bour, O., Paillet F.L and J-P. Caudal. 2006. Assessment of preferential flow
681 path connectivity and hydraulic properties at single-borehole and cross-borehole
682 scales in fractured aquifer. *J. of Hydrology*, 328, 347-359.

683 Leveinen, J., E. Rönkä, J. Tikkanen and E. Karro. 1998. Fractional flow dimensions and
684 hydraulic properties of a fracture-zone aquifer, Leppävirta, Finland. *Hydrogeology J.*,
685 vol.6, 327-340.

686 Lods, G. and Ph. Gouze. 2004. WTFM, software for Well Test analysis in Fractured Media
687 combining fractional flow with double porosity and leakance approaches. *Computer &*
688 *Geosciences Journal*. 937-947.

689 Loke M.H., Barker R.D., 1996. Rapid least-squares inversion of apparent resistivity
690 pseudosections using a quasi-Newton method. *Geophysical Prospecting*, 44, 131-152.

691 Mabee, S.B., Hardcastle, K.C. and Wise, D.U., 1994. A method of collecting and analyzing
692 lineaments for regional scale fissured-bedrock aquifer studies. *Ground Water*, 32(4),
693 pp.884-894.

694 Maréchal J.C., B. Dewandel, and K. Subrahmanyam. 2004. Use of hydraulic tests at
695 different scales to characterize fracture network properties in the weathered-fissured
696 layer of a hard rock aquifers. *Water Resources Res., vol.40, W11508*.

697 Maréchal, J.C., B. Dewandel, S. Ahmed, L. Galeazzi, 2006. Combining the groundwater
698 budget and water table fluctuation methods to estimate specific yield and natural
699 recharge. *Journal of Hydrology*, 329, 1-2, 281-293, doi:10.1016/j.jhydrol.2006.02.022.

700 Maréchal, J-C., Dewandel, B., Ahmed S. and P. Lachassagne, 2007. Hard-rock aquifers
701 characterization prior to modelling at catchment scale: an application to India. In:
702 Krásný J. – Sharp J.M. (eds.): *Groundwater in fractured rocks, IAH Selected Papers*,
703 9, 1-30. Taylor and Francis.

704 Meier, P.M., Carrera, J., and X. Sánchez-Vila, 1998. An evaluation of Jacob's method for
705 the interpretation of pumping tests in heterogeneous formations. *Water Resources*
706 *Research*, 34 (5), 1011-1025.

707 Nahon, D. B. 1991. Introduction to the Petrology of Soils and Chemical Weathering. Ed.
708 Wiley.

709 Neuman, S.P., Walter G.R., Bentley H.W., Ward J.J. and D.D. Gonzalez. 1984.
710 Determination of horizontal aquifer anisotropy with three wells. Ground Water, 22-1,
711 66-72.

712 Omorinbola, E.O. 1982. Verification of some geomorphological implcations of deep
713 weathering in the basement complex of Nigeria. *Journal of Hydrology*, 56, 347-368.

714 Owoade, A. 1995. The potential for minimizing drawdowns in groundwater wells in tropical
715 aquifers. *Journ. of African Earth Sciences*, 20, 3-4, 289-293.

716 Pickens, J.F., Grisak, G.E., Avis, J.D., Belanger, D.W. and Thury, M. 1987. Analysis and
717 interpretation of borehole hydraulic tests in deep boreholes; principles model
718 development, and applications. *Water Resources Res.*, vol. 23(7), pp.1341-1375.

719 Ramey, H.J. 1975. Interference analysis for anisotropic formations – a case history. *Jour. of*
720 *Petroleum Technology.*, 1290-1298.

721 Renard, Ph., Glenz D. and M. Mejias. 2009. Understanding diagnostic plots for well-test
722 interpretation. *Hydrogeology Journal*, 17, 589-600.

723 Sánchez-Vila, X., Meier, P.M. and J. Carrera, 1999. Pumping tests in heterogeneous
724 aquifers: an analytical study of what can be obtained from their interpretation using
725 Jacob's method. *Water Resources Research*. 35 (4), 943-952.

726 Sander P, Minor TB, Chesley M.M. 1997. Groundwater exploration based on lineament
727 analysis and reproducibility tests. *Ground Water* 35(5):888–894.

728 Sander P. 2007. Lineaments in groundwater exploration: a review of applications and
729 limitations.- *Hydrogeology Journal*, 15(1), 71-74.

730 Schad, H. and G. Teutsch, 1994. Effects of the investigation scale on pumping test results in
731 heterogeneous porous aquifers. *Journal of Hydrology*, 159, 61-77.

732 Spane F.A. and Wurstner S.K., 1993. DERIV: a computer program for calculating pressures
733 derivatives fir use in hydraulic test analysis. *Ground Water* 31:814–822.

734 Tardy, Y., 1971. Characterization of the principal weathering types by the geochemistry of
735 waters from some European and African crystalline massifs. *Chemical Geology*, vol.7,
736 253-271.

737 Tardy, Y. 1993. Pétrologie des latérites et des sols tropicaux.- 459 pp.- Masson, Paris.

738 Tardy, Y. 1998. Dérive des continents, latérites et paléoclimats tropicaux.- 472 pp.-
739 Editions BRGM, Orléans.

740 Taylor, R., and K. Howard. 2000. A tectono-geomorphic model of the hydrogeology of
741 deeply weathered crystalline rock: evidence from Uganda. *Hydrogeology J.*, *8*(3), 279-
742 294.

743 Uhl, V.W. and G.K. Sharma. 1978. Results of pumping tests in crystalline-rock aquifers.
744 *Ground Water*, vol.16 (3), pp. 192-203.

745 Walker, D.D., Gylling, B., Strom, A. and J.O. Selroos. 2001. Hydrogeologic studies for
746 nuclear-waste disposal in Sweden. *Hydrogeology J.*, vol.9(5), pp.419-431.

747 Wyns, R., J.-C. Gourry, J.-M. Baltassat, and F. Lebert. 1999. Caractérisation
748 multiparamètres des horizons de subsurface (0-100 m) en contexte de socle altéré, in
749 *2ème Colloque GEOFCAN*, edited by BRGM, IRD, UPMC, pp. 105-110, Orléans,
750 France.

751 Wyns, R., J. M. Baltassat, P. Lachassagne, A. Legchenko, J. Vairon, and F. Mathieu. 2004.
752 Application of SNMR soundings for groundwater reserves mapping in weathered
753 basement rocks (Brittany, France), *Bulletin de la Société Géologique de France*, 175
754 (1), pp. 21-34.
755

## Figure captions

Figure 1. Idealized weathering profile in hard-rock intersected by the current topography. The insert presents the area of interest of the paper: geological discontinuities (Wyns et al., 1999).

Figure 2. Location of the studied area with main geological features (G.S.I., 2002); Maheshwaram area, Ranga Reddy District, Andhra Pradesh, India.

Figure 3. Geological information and borehole locations. (a) IFP1 and (b) Kothur pilot sites. Lines A, B and C materialize the cross sections (see Figs. 6), and the other dotted lines the location of electrical-resistivity profiles (identical to line A for IFP1 site). Grey curves: soil elevation (masl). BW: farmer's wells.

Figure 4. Interpreted geological cross sections. (a) perpendicular to the quartz reef at IFP1 site, (b) perpendicular and (c) parallel to the quartz reef at Kothur site. Location of the cross sections is shown on Figure 3 (lines A, B and C).

Figure 5. Histogram on a logarithmic scale of the hydraulic conductivity deduced from slug tests analysis. The data from the boreholes located in the quartz reef (average: LogK: -5.58 ±1.0; number of data [n]: 6) and in the granite surrounding the reef (average: LogK: -5.62 ±0.6; n: 15) are compared to the granite far from discontinuities (average: LogK: -5.36 ±1.0, n: 30; Maheshwaram area [same area] Maréchal et al., 2004). LogK: natural logarithm of hydraulic conductivity.

Figure 6. Observed and modelled drawdowns and derivatives. (a) Pumping well IFP30-5 and observation well IFP30-2; model: Hantush (WinIsape software). (b) Pumping well IFP30-10, and observation wells IFP30-5 and IFP30-.6; model: dual porosity. IFP 30-6 considers the response of the matrix (WTFM software) (c) Pumping well IFP1-6 and observation well IFP1-9; model: Theis+2 no-flow boundaries (WinIsape software).

Figure 7. Heterogeneity in hydraulic conductivity on the horizontal plane. (a) Pumping at IFP30-5; hydraulic conductivity from Table 3. (b) Pumping at IFP30-10; hydraulic conductivity from Table 4. (c) Pumping at IFP1-6; hydraulic conductivity from Table 6.

Circles: wells located in the quartz reef; triangles: wells located in the granite. Error bars depict the range of the estimates deduced from the drawdown curve interpretations. $\alpha$: angle between *Ky* and *Kmax*.

Figure 8. Idealized conceptual hydrodynamic model of the aquifer associated to the quartz reef. Data from the horizontal stratiform fissured layer are from Maréchal et al. (2004) and Dewandel et al. (2006).

## Table captions

Table 1. Characteristics of the wells in the IFP1 and Kothur sites and hydraulic conductivity (K) deduced from slug tests.

Table 2. Characteristics of pumping tests performed at the IFP1 and Kothur pilot sites. * Geology of the aquifer zone; ** drawdown at the end of pumping, and *** number of observation wells that reacted to pumping. The diagnoses are deduced from derivative curve analyses.

Table 3. Results of the interpretation of the pumping in IFP30-5 (Kothur site; quartz aquifer). Model: Hantush (partially penetrating well). * drawdown at the end of pumping, ** K and S are geometrical mean; others are arithmetic mean, and *** estimated from geological logs. StDev.: standard deviation.

Table 4. Results of the interpretation of pumping in IFP30-10 (Kothur site; quartz aquifer). Model: dual-porosity. * observation well interpreted in the matrix, ** drawdown at the end of pumping, and *** geometrical mean.

Table 5. Results of the interpretation of the pumping in IFP30-4 (Kothur site; granite aquifer). Model: dual-porosity. * drawdown at the end of pumping, and ** geometrical mean.

Table 6. Results of the interpretations of pumping in IFP1-6 (IFP1 site; granite aquifer). Model: Theis + two no-flow boundaries. * drawdown at the end of pumping, ** estimated

822 using the average S (7.8E-4), *** the number between comas is estimated using the average S
823 and **** K and S are geometrical mean, do not include data from observation wells IFP 1-3,
824 1-4 and 1-8 (located in another aquifer); distances to limits are arithmetic mean.
825
826

# Tables

| Well ID | site | Depth (m) | Casing depth (m) | Main Geology | Saprolite thickness -granite (m) | Highly weathered quartz (m) | Basement depth (m) | K_slug (m/s) |
|---|---|---|---|---|---|---|---|---|
| IFP1 | IFP1 | 42.0 | 8.8 | Granite | 18.3 | - | 37.5 | 7.4E-06 |
| IFP1-1 | IFP1 | 59.5 | 5.8 | Granite | 15.5 | - | 51 | 3.2E-06 |
| IFP1-2 | IFP1 | 35.0 | 12 | Granite | 22.5 | - | 30.2 | 7.4E-06 |
| IFP1-3 | IFP1 | 35.0 | 5.7 | Granite | 17 | - | 29 | 4.4E-07 |
| IFP1-4 | IFP1 | 68.6 | 6 | Dolerite+granite | no data | - | 77.7 | 7.6E-07 |
| IFP1-5 | IFP1 | 73.2 | 11.6 | Granite | | 9 | 32 | 2.9E-06 |
| IFP1-6 | IFP1 | 73.2 | 22.9 | Granite | 13.5 | 2.5 (overlying the saprolite) | 51 | 3.1E-06 |
| IFP1-7 | IFP1 | 59.4 | 27.1 | Granite | 11.5 | | 44 | 3.9E-06 |
| IFP1-8 | IFP1 | 54.9 | 11.6 | Dolerite+granite | 7 m of highly weathered dolerite (clay) | | 41 | 6.5E-06 |
| IFP1-9 | IFP1 | 59.4 | 18.3 | Granite | 12.8 | | 49 | 6.0E-06 |
| IFP30-1 | Kothur | 91.4 | 11.6 | Quartz | | 6.5 | 91.4 | 5.6E-07 |
| IFP30-2 | Kothur | 45.7 | 29.9 | Granite | 20.6 | 4.0 (overlying saprolite) | 41 | 2.8E-06 |
| IFP30-3 | Kothur | 50.3 | 29.9 | Granite | 27.1 | 2.7 (overlying saprolite) | 36.5 | 8.5E-08 |
| IFP30-4 | Kothur | 50.3 | 29.9 | Granite | 29.2 | | 42 | 8.8E-06 |
| IFP30-5 | Kothur | 77.7 | 17.4 | Quartz | | 20.2 | 77.7 | 5.1E-06 |
| IFP30-6 | Kothur | 50.3 | 11.6 | Quartz | | 6.8 | 50.3 | 5.1E-08 |
| IFP30-7 | Kothur | 64.0 | 30.2 | Granite | 16.7 | 8.8 (overlying saprolite) | 51.5 | 4.5E-07 |
| IFP30-8 | Kothur | 50.0 | 42.7 | Granite | 28 | | 38 | 6.3E-06 |
| IFP30-9 | Kothur | 59.4 | 30.5 | Quartz | | 39.5 | 50 | 1.1E-05 |
| IFP30-10 | Kothur | 73.0 | 27.4 | Quartz | | 30 | 73 | 1.6E-05 |
| IFP30-11 | Kothur | 74.0 | 12.2 | Quartz | | 25.5 | 36.5 | 1.30E-05 |

Table 1.

| Pumping Wells | Tested aquifer * | Well radius (m) | Pumping rate ($m^3/h$) | Duration of the test (min.) | Max. dd. (m)** | Nb. of obs. wells *** | Diagnosis |
|---|---|---|---|---|---|---|---|
| IFP1-6 | granite | 0.11 | 13.5 | 1580 | 21.48 | 9 | Channelized flow |
| IFP1-8 | granite | 0.11 | 3.5 | 1430 | 5.51 | 3 | One-no flow boundary |
| IFP30-4 | granite | 0.11 | 6.8 | 1440 | 10.31 | 2 | Dual porosity |
| IFP30-5 | quartz | 0.11 | 4.9 | 1440 | 8.33 | 7 | Partially penetrating well |
| IFP30-10 | quartz | 0.11 | 16.3 | 2890 | 9.9 | 8 | Dual porosity |

Table 2.

| Well ID | | r (m) | s-max* (m) | K (m/s) | S (-) | Anisotropy Kx/Kz (-) | Aquifer thickness (m) | Screened thickness (m)*** |
|---|---|---|---|---|---|---|---|---|
| IFP30-5 | pump. well | 0.11 | 8.33 | 4.2E-06 | - | 3.1 | 110 | 35 |
| IFP30-1 | obs.well | 30.1 | 1.12 | 3.6E-06 | 1.4E-03 | 3.5 | 140 | 10 |
| IFP30-2 | obs.well | 27.3 | 2.13 | 2.6E-06 | 4.0E-04 | 2.0 | 130 | 40 |
| IFP30-6 | obs.well | 96.2 | 0.44 | 3.4E-06 | 1.8E-03 | 3.0 | 130 | 20 |
| IFP30-7 | obs.well | 52.5 | 0.45 | 2.9E-06 | 7.5E-03 | 10.0 | 110 | 50 |
| IFP30-9 | obs.well | 88.0 | 1.18 | 5.1E-06 | 4.5E-05 | 1.0 | 100 | 100 |
| IFP30-10 | obs.well | 135.5 | 1.06 | 5.5E-06 | 2.7E-05 | 1.0 | 100 | 100 |
| IFP30-11 | obs.well | 180.6 | 0.85 | 5.9E-06 | 3.5E-05 | 1.0 | 100 | 100 |
| IFP30-3 | obs.well | 62.5 | No reaction | - | - | - | - | - |
| IFP30-4 | obs.well | 103.0 | No reaction | - | - | - | - | - |
| IFP30-8 | obs.well | 118.0 | No reaction | - | - | - | - | - |
| | | | Average** | 4.0E-06 | 3.2E-04 | 3.1 | 115.0 | |
| | | | Std.Dev (±) | 1.2E-06 | 2.7E-03 | 3.0 | 16.0 | |

Table 3.

| Well | | r (m) | s-max** (m) | Kf (m/s) | Km (m/s) | Sf (-) | Sm (-) | Stot (-) |
|---|---|---|---|---|---|---|---|---|
| IFP30/10 | pump. well | 0.11 | 9.9 | 6.3E-06 | 2.4E-09 | - | - | - |
| IFP30/1 | obs.well | 123.2 | 3.38 | 8.5E-06 | 4.5E-10 | 4.9E-05 | 6.1E-05 | 1.1E-04 |
| IFP30/2 | obs.well | 115.1 | 3.63 | 6.5E-06 | 1.9E-09 | 4.2E-05 | 1.8E-04 | 2.2E-04 |
| IFP30/5 | obs.well | 135.7 | 4.42 | 6.5E-06 | 6.0E-10 | 1.5E-05 | 4.9E-05 | 6.4E-05 |
| IFP30/6* | obs.well | 222.0 | 1.27 | 1.1E-05 | 1.5E-09 | 8.5E-05 | 1.3E-04 | 2.1E-04 |
| IFP30/7* | obs.well | 145.0 | 1.04 | 6.0E-06 | 8.0E-09 | 2.4E-04 | 2.2E-03 | 2.5E-03 |
| IFP30/8 | obs.well | 92.0 | 0.18 | 2.1E-06 | 2.6E-08 | 4.9E-03 | 6.1E-02 | 6.6E-02 |
| IFP30/9 | obs.well | 49.4 | 5.5 | 6.5E-06 | 1.4E-09 | 2.6E-05 | 1.2E-04 | 1.5E-04 |
| IFP30/11 | obs.well | 57.8 | 4.97 | 6.2E-06 | 5.5E-09 | 5.2E-05 | 1.9E-04 | 2.4E-04 |
| IFP30/3 | obs.well | 132.8 | No reaction | - | - | - | - | - |
| IFP30/4 | obs.well | 144.5 | No reaction | - | - | - | - | - |
| | | | geomean*** | 6.2E-06 | 2.4E-09 | 8.9E-05 | 3.5E-04 | 4.6E-04 |
| | | | StDev (±) | 2.4E-06 | 8.2E-09 | 1.7E-03 | 2.1E-02 | 2.3E-02 |

Table 4.

| Well | WTFM | r (m) | s-max* (m) | Kf (m/s) | Km (m/s) | Sf (-) | Sm (-) | Stot (-) |
|---|---|---|---|---|---|---|---|---|
| IFP30/4 | pump. well | 0.11 | 10.31 | 6.4E-06 | 4.0E-09 | - | - | - |
| IFP30/3 | obs.well | 40.6 | 1.08 | 6.5E-06 | 7.0E-09 | 9.5E-05 | 6.7E-03 | 6.8E-03 |
| IFP30/8 | obs.well | 59.8 | 0.52 | 6.3E-06 | 9.0E-10 | 1.6E-04 | 7.6E-03 | 7.8E-03 |
| | | | geomean** | 6.4E-06 | 2.9E-09 | 1.2E-04 | 7.1E-03 | 7.2E-03 |
| | | | StDev (±) | 1.0E-07 | 3.0E-09 | 4.5E-05 | 6.7E-04 | 7.2E-04 |

Table 5.

859

| | | | | | | NO flow Limit_d1 | NO flow Limit_d2 |
|---|---|---|---|---|---|---|---|
| Well ID | | r (m) | s-max* | K (m/s) | S (-) | dist. (m) | dist. (m) |
| IFP1-6 | pump. well | 0.11 | 21.48 | 5.1E-06 | - | *20* ** | *46*** |
| IFP1 | obs.well | 18.6 | 20.28 | 4.0E-06 | 7.0E-05 | 31 *(10)**** | 138 *(41)**** |
| IFP1-1 | obs.well | 28.2 | 11.87 | 6.0E-06 | 4.2E-04 | 35 | 47 |
| IFP1-2 | obs.well | 40.4 | 9.28 | 5.4E-06 | 1.6E-04 | - | 42 |
| IFP1-5 | obs.well | 17.7 | 12.69 | 7.9E-06 | 1.7E-02 | 25 | 44 |
| IFP1-7 | obs.well | 8.7 | 14.05 | 3.3E-06 | 1.1E-03 | 16 | - |
| IFP1-9 | obs.well | 11.5 | 16.44 | 3.0E-06 | 2.6E-03 | 13 | 42 |
| IFP1-3 | obs.well | 61.5 | 0.75 | 3.3E-06 | 8.3E-04 | 18 | 43 |
| IFP1-4 | obs.well | 40.4 | 0.3 | *4.8E-05* | *2.6E-02* | - | - |
| IFP1-8 | obs.well | 51.7 | 0.1 | *1.0E-04* | *6.3E-02* | | - |
| BW1 | obs.well | 69.3 | No reaction | - | - | - | - |
| BW2 | obs.well | 95.4 | No reaction | - | - | - | - |
| | | | Average**** | 4.5E-06 | 7.8E-04 | 19.5 | 44.3 |
| | | | StDev (±) | 1.7E-06 | 6.0E-03 | 8.8 | 2.1 |

860

861 Table 6.

862

## Figures

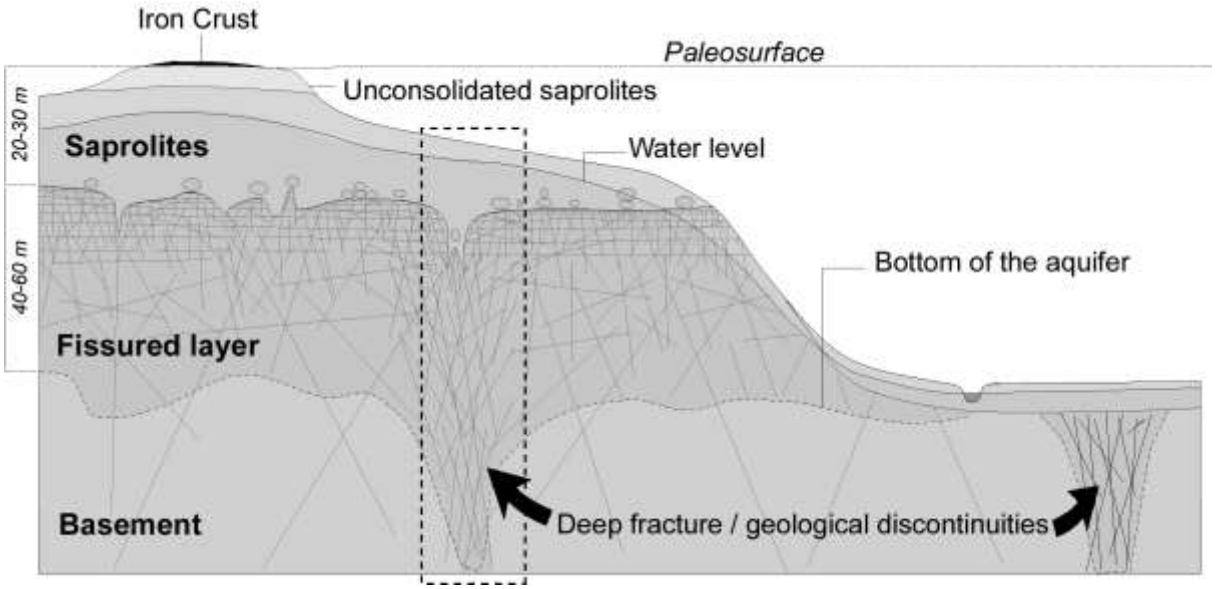


Figure 1

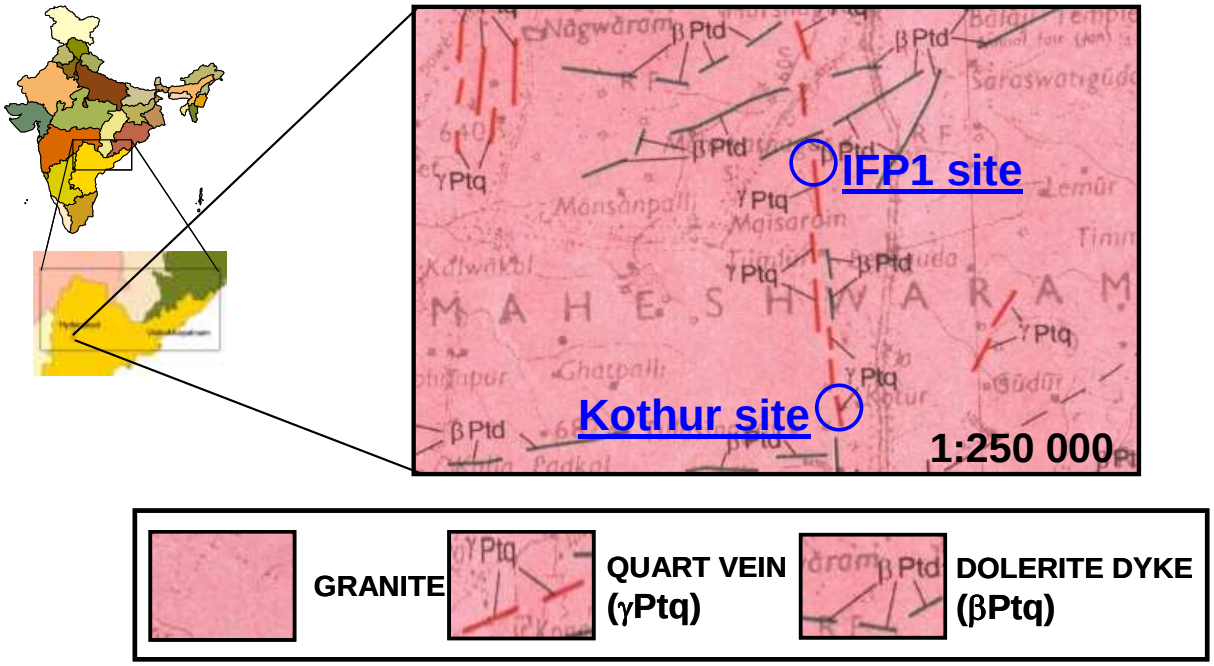


Figure 2

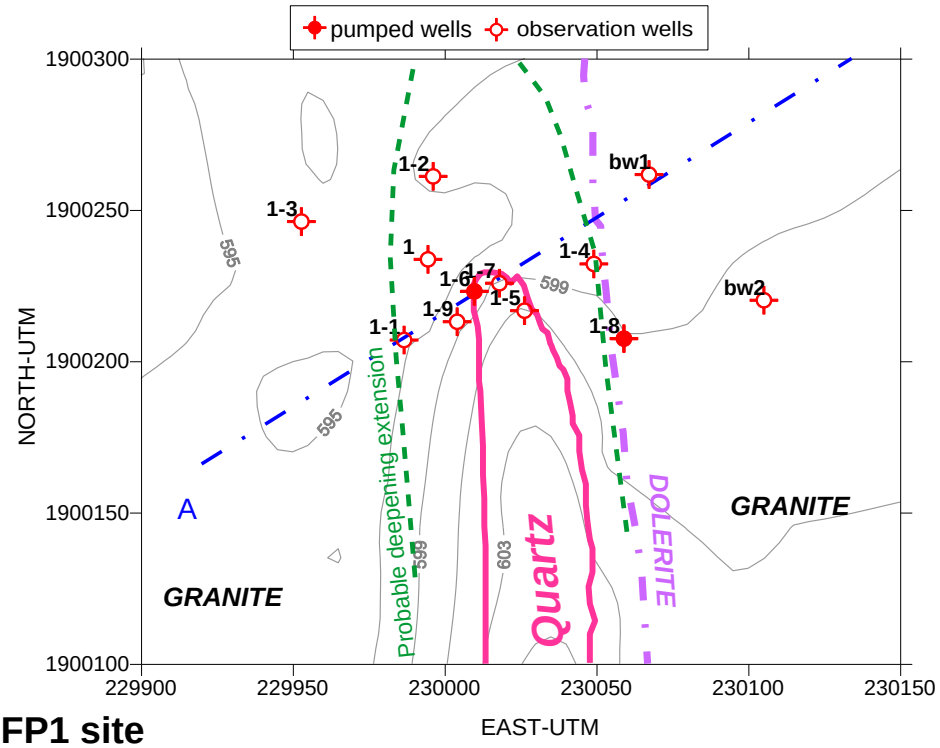


**a) IFP1 site**

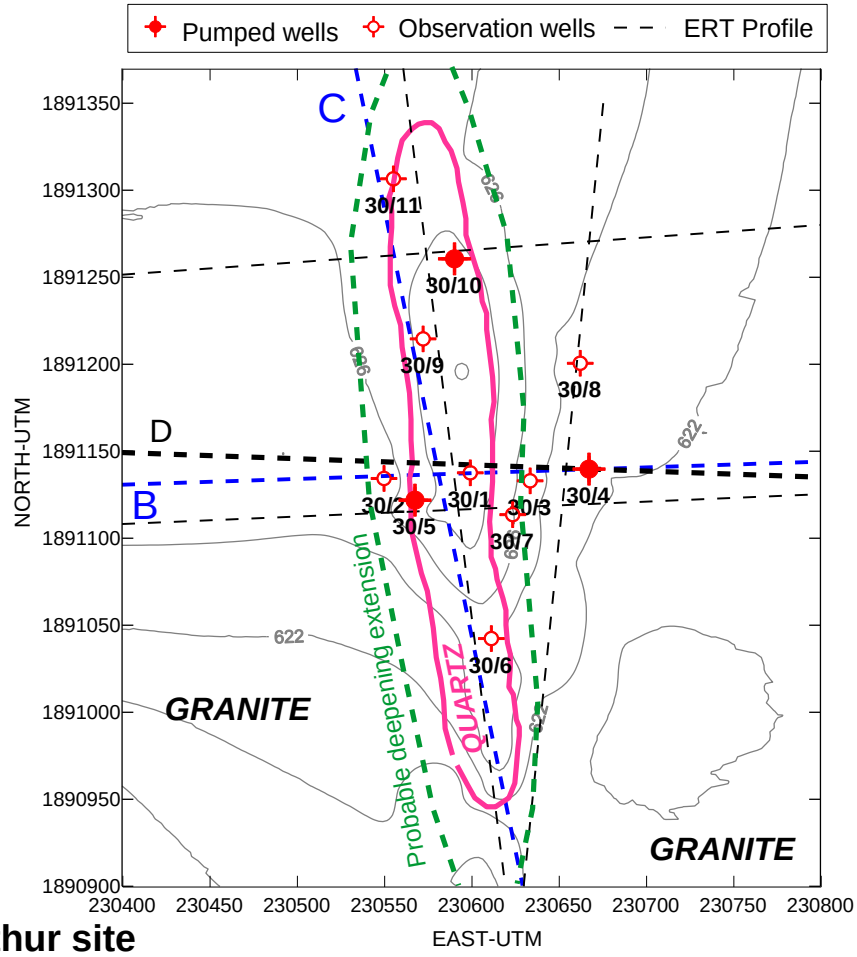


**b) Kothur site**

Figure 3

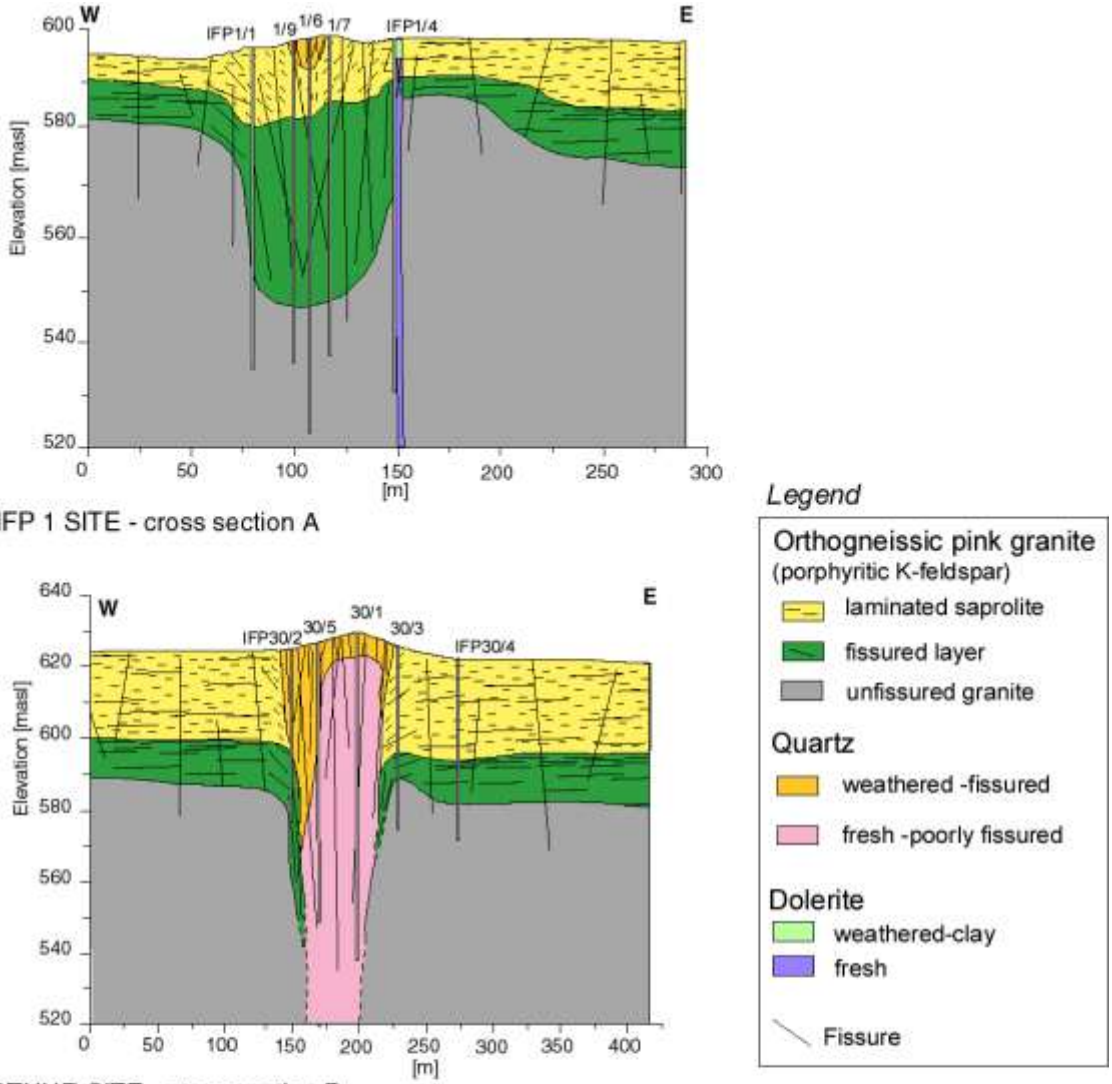
W
E
IFP1/1
1/9
1/6
1/7
IFP1/4
Elevation [masl]
600
580
560
540
520
0
50
100
150
200
250
300
[m]
a) IFP 1 SITE - cross section A
W
E
IFP30/2
30/5
30/1
30/3
IFP30/4
640
620
600
580
560
540
520
0
50
100
150
200
250
300
350
400
[m]
b) KOTHUR SITE - cross section B
N
S
IFP 30/11
IFP30/9
IFP30/5
IFP30/6
640
620
600
580
560
540
520
0
50
100
150
200
250
300
350
400
450
[m]
c) KOTHUR SITE - cross section C
Legend
Orthogneissic pink granite
(porphyritic K-feldspar)
laminated saprolite
fissured layer
unfissured granite
Quartz
weathered -fissured
fresh -poorly fissured
Dolerite
weathered-clay
fresh
Fissure

Figure 4.

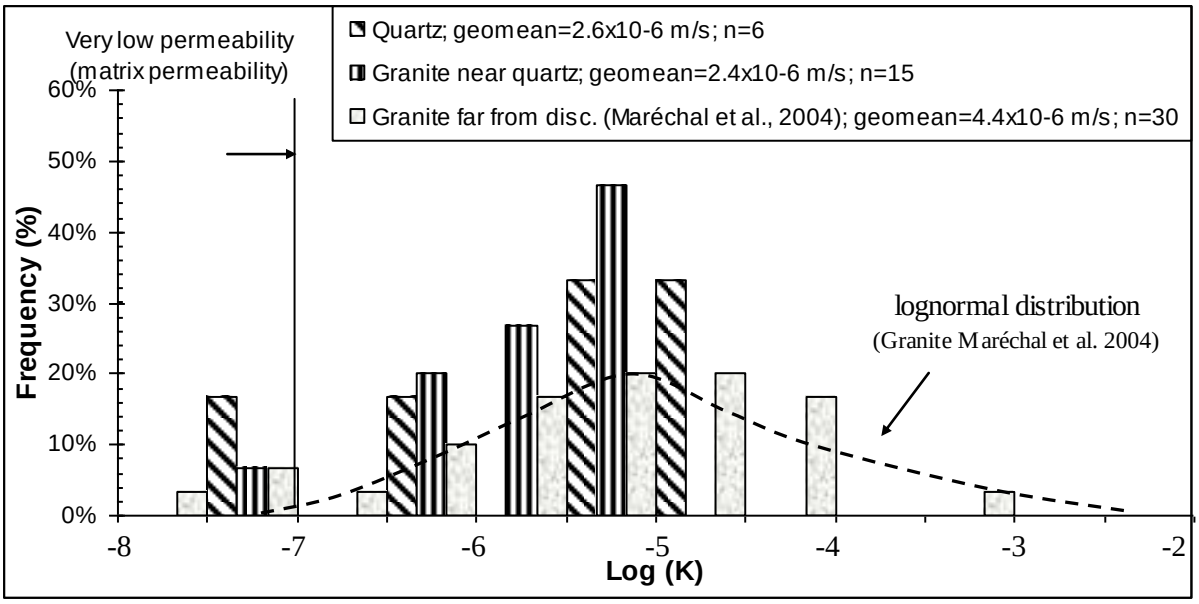
Very low permeability
(matrix permeability)
Quartz; geomean=2.6x10-6 m/s; n=6
Granite near quartz; geomean=2.4x10-6 m/s; n=15
Granite far from disc. (Maréchal et al., 2004); geomean=4.4x10-6 m/s; n=30
lognormal distribution
(Granite Maréchal et al. 2004)
Frequency (%)
60%
50%
40%
30%
20%
10%
0%
-8
-7
-6
-5
-4
-3
-2
Log (K)

Figure 5.

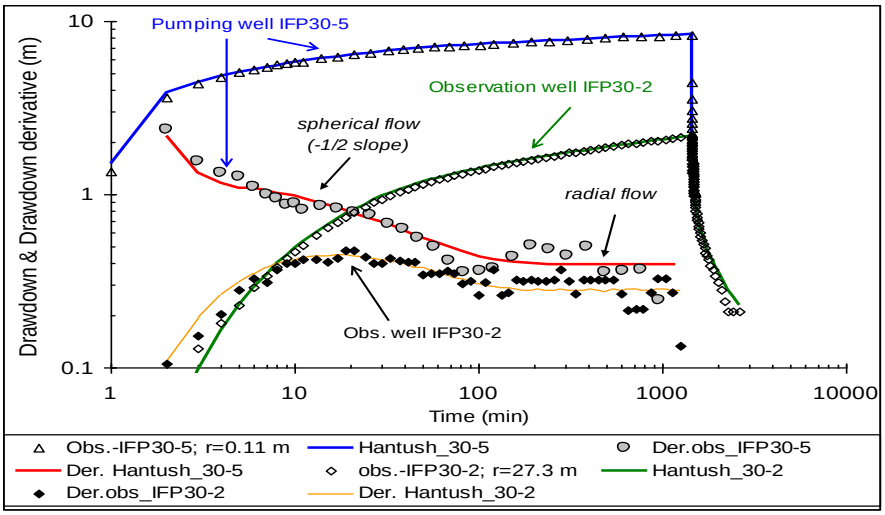


**a) IPF30-5**

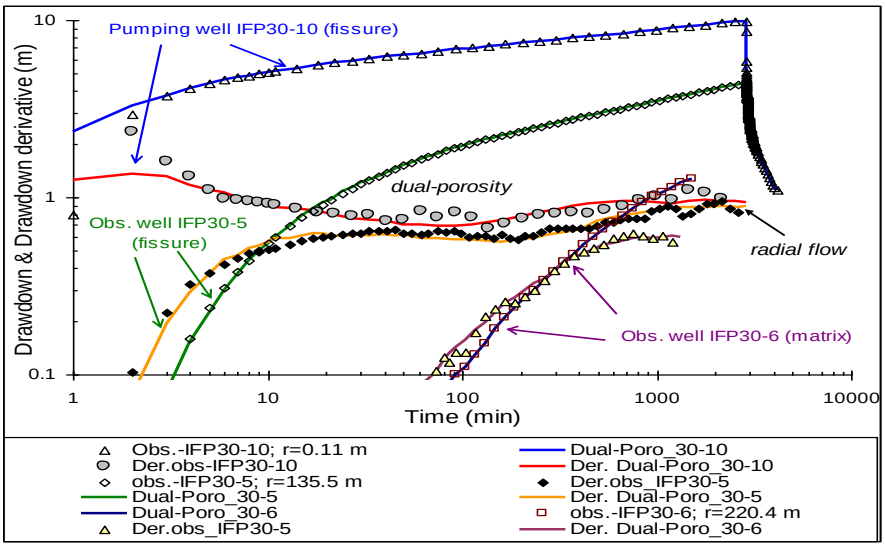


**b) IPF30-10**

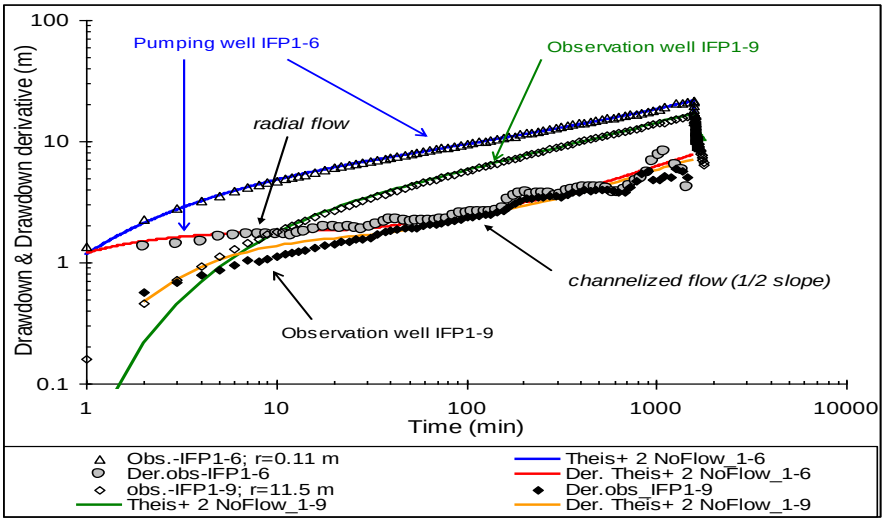


**c) IPF1-6**

Figure 6.

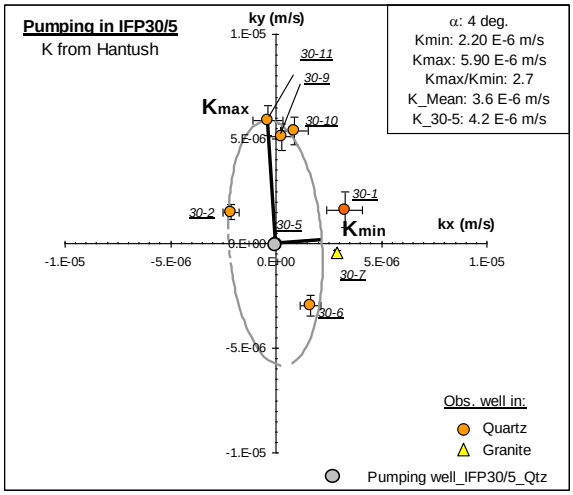


**a) IFP30-5 –Kothur site**

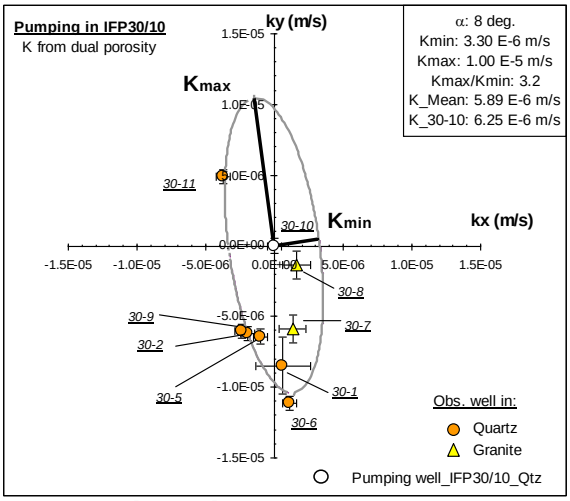


**b) IFP30-10 –Kothur site**

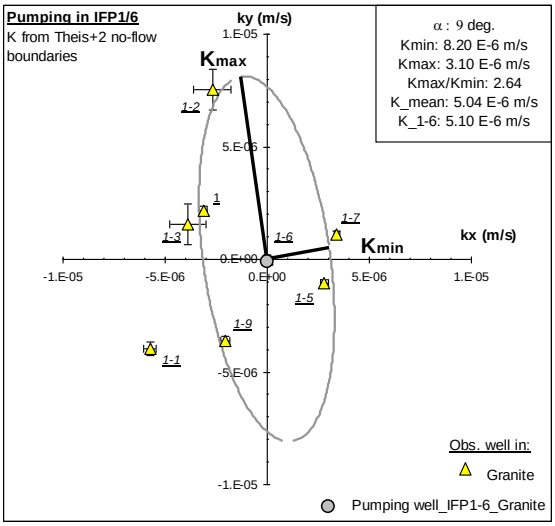


**c) IFP1-6 –IFP1 site**

Figure 7.

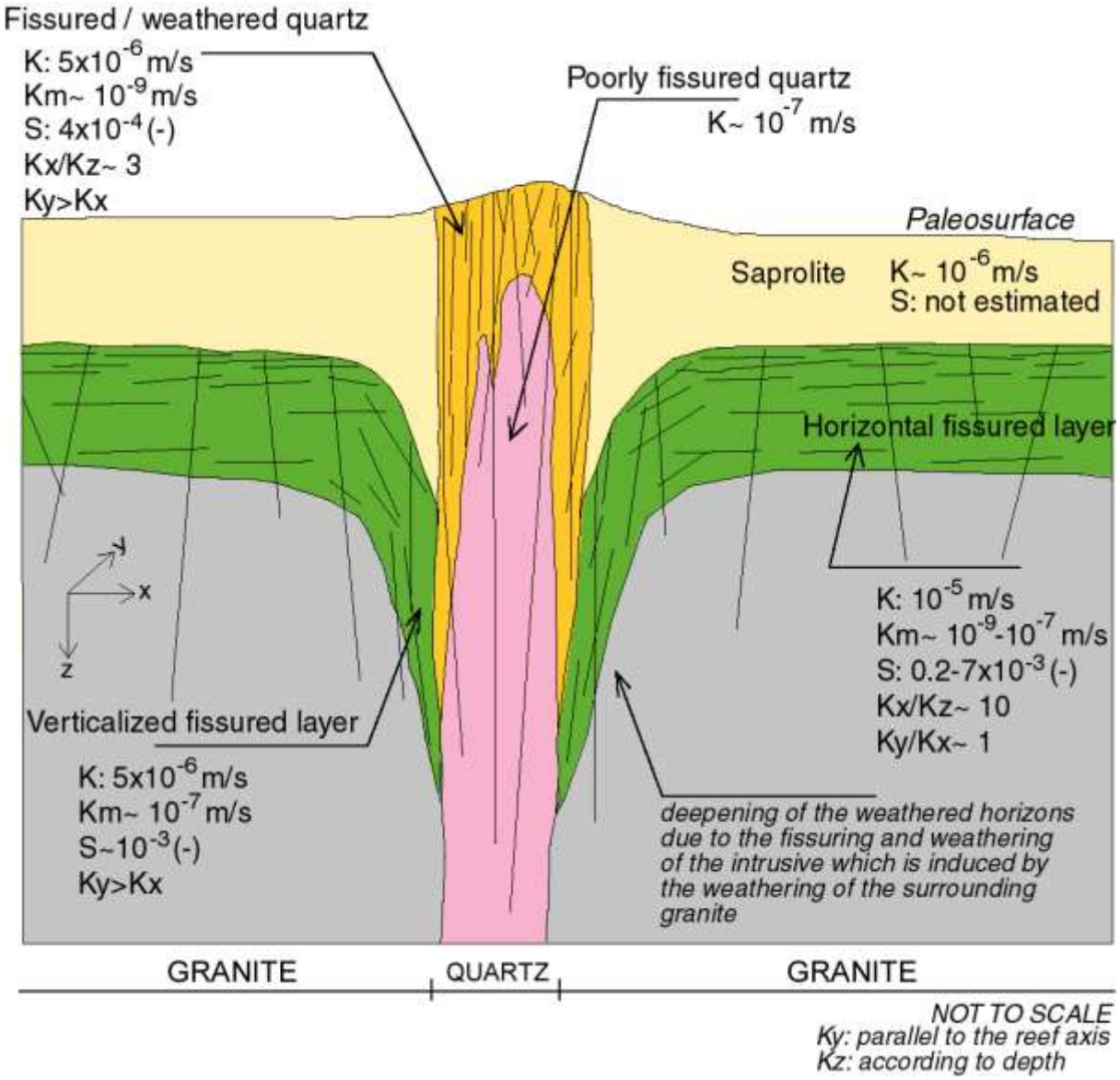
Fissured / weathered quartz
K: 5x10-6 m/s
Km~ 10-9 m/s
S: 4x10-4 (-)
Kx/Kz~ 3
Ky>Kx
Poorly fissured quartz
K~ 10-7 m/s
Paleosurface
Saprolite
K~ 10-6 m/s
S: not estimated
Horizontal fissured layer
K: 10-5 m/s
Km~ 10-9-10-7 m/s
S: 0.2-7x10-3 (-)
Kx/Kz~ 10
Ky/Kx~ 1
Verticalized fissured layer
K: 5x10-6 m/s
Km~ 10-7 m/s
S~10-3 (-)
Ky>Kx
deepening of the weathered horizons due to the fissuring and weathering of the intrusive which is induced by the weathering of the surrounding granite
y
x
z
GRANITE
QUARTZ
GRANITE
NOT TO SCALE
Ky: parallel to the reef axis
Kz: according to depth

Figure 8.